A Noninvasive Method for Quantifying Cerebral Metabolic Rate of Oxygen by Hybrid PET/MRI: Validation in a Porcine Model

Lucas Narciso[1,2], Tracy Ssali[1,2], Linshan Liu[1], Heather Biernaski[1], John Butler[1], Laura Morrison[1], Jennifer Hadway[1], Jeffrey Corsaut[1], Justin W. Hicks[1,2], Michael C. Langham[3], Felix W. Wehrli[3], Hidehiro Iida[4,5], and Keith St Lawrence[1,2]

[1]Lawson Health Research Institute, London, Ontario, Canada; [2]Department of Medical Biophysics, Western University, London, Ontario, Canada; [3]Department of Radiology, University of Pennsylvania Perelman School of Medicine, Philadelphia, Pennsylvania; [4]University of Turku and Turku PET Centre, Turku, Finland; and [5] National Cerebral and Cardiovascular Center, Suita, Osaka, Japan

The gold standard for imaging the cerebral metabolic rate of oxygen ($CMRO_2$) is PET; however, it is an invasive and complex procedure that also requires correction for recirculating ^{15}O-H_2O and the blood-borne activity. We propose a noninvasive reference-based hybrid PET/MRI method that uses functional MRI techniques to calibrate ^{15}O-O_2 PET data. Here, PET/MRI of oxidative metabolism (PMROx) was validated in an animal model by comparison to PET-alone measurements. Additionally, we investigated if the MRI perfusion technique arterial spin labeling (ASL) could be used to further simplify PMROx by replacing ^{15}O-H_2O PET, and if the PMROx was sensitive to anesthetic-induced changes in metabolism. **Methods:** ^{15}O-H_2O and ^{15}O-O_2 PET data were acquired using a hybrid PET/MR scanner, together with simultaneous functional MRI (OxFlow and ASL), from juvenile pigs ($n = 9$). Animals were anesthetized with 3% isoflurane and 6 mL/kg/h propofol for the validation experiments, and arterial sampling was performed for PET-alone measurements. PMROx estimates were obtained using whole-brain (WB) $CMRO_2$ from OxFlow and local cerebral blood flow (CBF) from either noninvasive ^{15}O-H_2O PET or ASL ($PMROx_{ASL}$). Changes in metabolism were investigated by increasing the propofol infusion to 20 mL/kg/h. **Results:** Good agreement and correlation were observed between regional $CMRO_2$ measurements from PMROx and PET alone. No significant differences were found between OxFlow and PET-only measurements of WB oxygen extraction fraction (0.30 ± 0.09 and 0.31 ± 0.09) and CBF (54.1 ± 16.7 and 56.6 ± 21.0 mL/100 g/min), or between PMROx and PET-only $CMRO_2$ estimates (1.89 ± 0.16 and 1.81 ± 0.10 mLO_2/100 g/min). Moreover, PMROx and $PMROx_{ASL}$ were sensitive to propofol-induced reduction in $CMRO_2$. **Conclusion:** This study provides initial validation of a noninvasive PET/MRI technique that circumvents many of the complexities of PET $CMRO_2$ imaging. PMROx does not require arterial sampling and has the potential to reduce PET imaging to ^{15}O-O_2 only; however, future validation involving human participants are required.

Key Words: cerebral blood flow; cerebral metabolic rate of oxygen; noninvasive PET; oxygen extraction fraction; PET/MRI

J Nucl Med 2021; 62:1789–1796
DOI: 10.2967/jnumed.120.260521

PET imaging of cerebral oxidative metabolism was developed over 30 y ago and continues to prove a vital tool for understanding brain energetics and the role of altered metabolism in disease processes (*1–3*). PET remains the gold standard for imaging the cerebral metabolic rate of oxygen ($CMRO_2$); however, the original procedure is complex and long (*4*). In addition to radiolabeled oxygen, ^{15}O-H_2O is needed to measure cerebral blood flow (CBF) and ^{15}O-CO to measure the cerebral blood volume (CBV). Arterial blood sampling is required for each tracer, along with separating plasma and red blood cell activity for ^{15}O-O_2 to account for the increasing signal contribution from metabolically generated ^{15}O-H_2O (recirculating water, RW). Efforts to reduce the complexity and duration of the original procedure have led to modeling approaches that eliminate the need for separate CBV imaging and estimating RW without separating blood samples (*5*). Alternately, the effects of RW can be minimized by short scan times after a single inhalation of ^{15}O-O_2 (*6*). More recently, approaches incorporating image-derived input functions have been proposed to avoid measuring the arterial input function (AIF), which is an invasive and inherently noisy procedure (*7*,*8*). However, the accuracy of these approaches depends on either an empiric factor relating the total AIF and its RW component, or careful measurement of a coefficient to scale the arterial time–activity curve.

We propose an alternative method to reduce the complexity, invasiveness, and duration of $CMRO_2$ imaging (*9*). Similar to Su et al. (*8*), this method takes advantage of simultaneous PET/MRI. However, rather than attempting to use MRI to help extract the AIF, the proposed hybrid approach incorporates complementary MRI techniques to measure whole-brain (WB) $CMRO_2$ to serve as a reference to calibrate dynamic ^{15}O-oxygen PET data. Analogous to a similar PET/MR technique for imaging CBF (*10*), this hybrid approach eliminates the need for arterial sampling. Here, we implemented this reference-based approach, hereafter referred as PMROx (PET/MRI of oxidative metabolism), on a 3-T PET/MR scanner. The aim of this study was to validate PMROx in a large animal model by comparison with a previously validated dual-basis function method (DBFM) (*11*). In addition, we investigated if PMROx could be further simplified by incorporating CBF images from the MRI-based technique arterial spin labeling (ASL). This modification reduces PET imaging to only ^{15}O-O_2 and imaging duration to approximately 5 min since the MRI sequences can be run during the PET acquisition (*12*). In addition to validating PMROx, its

Received Nov. 19, 2020; revision accepted Mar. 5, 2021.
For correspondence or reprints, contact Lucas Narciso (lnarciso@uwo.ca) and Keith St Lawrence (kstlaw@lawsonimaging.ca).
Published online March 19, 2021.

sensitivity to changes in metabolism was investigated by altering the anesthetics administered to the animals.

MATERIALS AND METHODS

Animal experiments were conducted according to the regulations of the Canadian Council of Animal Care and approved by the Animal Care Committee at Western University. Before imaging, juvenile Duroc pigs were tracheotomized, and catheters were inserted into the cephalic veins and femoral arteries. During imaging, animals were mechanically ventilated, immobilized on a custom platform, and anesthetized with 3% isoflurane and 6 mL/kg/h propofol. Blood samples were collected to measure the partial pressures of oxygen and carbon dioxide, plasma glucose concentration, hematocrit, and hemoglobin concentration. Throughout the experiment, end-tidal O_2 and CO_2, temperature, heart rate, and oxygen saturation were monitored to ensure normal levels.

Study Protocol

PET and MRI data were obtained on a 3-T Siemens Biograph mMR system using a 12-channel PET-compatible receiver head coil (Siemens GmbH). Each experiment was divided into 2 parts. First, the accuracy of PMROx was evaluated by comparing with the DBFM, which required measuring the AIFs of ^{15}O-H_2O and ^{15}O-O_2. Next, the sensitivity of PMROx to the expected reduction in cerebral metabolism was assessed by increasing the infusion rate of propofol to 20 mL/kg/h to induce a lower metabolic condition (LMC).

In both parts, PET imaging involved injecting ^{15}O-H_2O to measure CBF, followed by inhalation of ^{15}O-O_2 to measure oxygen extraction fraction (OEF). Concurrently, WB $CMRO_2$ was obtained by the MRI sequence OxFlow (*13*), which combines phase-contrast MRI measurements of CBF from the internal carotid and basilar arteries, with venous oxygen saturation (S_vO_2) measurements from the superior sagittal sinus acquired with susceptibility-based oximetry (*14*). CBF images were collected using pseudocontinuous ASL (pCASL). At the end of the experiment, the animal was euthanized according to the animal care guidelines and transported to a CT scanner to obtain a postmortem CT-based attenuation correction map.

PET Imaging and Postprocessing

The PET protocol (Fig. 1) began with injection of ^{15}O-H_2O (460 ± 80 MBq; cephalic vein), followed by inhalation of 2,200 MBq of ^{15}O-O_2. All acquisitions involved 5 min of list-mode acquisition. For DBFM, AIFs from ^{15}O-H_2O ($C_a^w(t)$) and ^{15}O-O_2 ($C_a^o(t)$) were determined by withdrawing blood from a femoral artery and measuring the activity using an MR-compatible system (Swisstrace GmbH). ^{15}O-O_2 PET data acquisition during the LMC started approximately 1 h after the first ^{15}O-O_2 acquisition to allow the animal to stabilize after changing the anesthetics.

^{15}O-H_2O and ^{15}O-O_2 were produced by (d,n) ^{14}N reaction in an onsite cyclotron (PETtrace 800, 16.5 MeV; GE Healthcare) (*15*). For ^{15}O-O_2 imaging, the radioactive gas was filtered before being transferred to the PET/MR suite via a stainless-steel line (202-m long, 3-mm diameter). The line was connected to polyethylene tubing that directly fed into the inhalation tube of the animal (delivery rate of 1.5 L/min for 30 s). Expired gas was collected in a 200-L tank to hold it for 7 half-lives (*16*).

Dynamic PET images were reconstructed into 48 time frames (30 × 3, 6 × 5, 6 × 10, and 6 × 20 s) using the Siemens e7-tools suite with a 3-dimensional ordered subset expectation maximization method (iterations/subsets, 4/21; matrix size, 344 × 344 × 127 voxels; field of view [FoV], 359 × 359 × 258 mm^3; voxel size, 1 × 1 × 2 mm^3; zoom factor, 2). Raw data were corrected for decay, random incidences, dead-time, detector normalization, data rebinning, and scatter. Absolute scatter correction was used for the ^{15}O-O_2 images, as recommended for 3-dimensional scanning (*17*). Reconstructed images were smoothed by a 4-mm gaussian filter.

AIFs were decay corrected and denoised using a wavelet signal denoising function (MATLAB R2017b, Block James-Stein method). The RW ($A_w(t)$) component of the measured ^{15}O-O_2 AIF was estimated using species-specific values after interpolating to the differences in weight (*18*).

MR Imaging and Postprocessing

MR acquisition (Supplemental Fig. 1; supplemental materials are available at http://jnm.snmjournals.org) began with T1-weighted images (magnetization-prepared rapid gradient-echo sequence, MPRAGE; repetition/echo/inversion times [TR/TE/TI], 2,000/2.98/900 ms; flip angle [α], 9°; FoV, 256 × 256 mm^2; 176 slices; isotropic voxel size, 1 mm^3), followed by time-of-flight images to identify the feeding arteries for phase-contrast imaging (TR/TE, 22/3.75 ms; α, 18°; FoV, 200 × 181 mm^2; 102 slices; voxel size, 0.3 × 0.3 × 1.5 mm^3; 40 mm saturation band) and the sagittal sinus for oximetry imaging (no saturation band).

MR images acquired during PET acquisitions were OxFlow and pCASL. The former alternates between the 2 slice locations to measure WB CBF and S_vO_2 (TR/TE/ΔTE, 35/7.025/2.5 ms; α, 25°; FoV, 208 × 208 mm^2; voxel size, 1.6 × 1.6 × 5.0 mm^3; velocity encoding, 60 cm/s; acquisition time, 1 min) (*13*). The acquisition of the OxFlow sequence was timed to coincide with the ^{15}O-O_2 imaging, and the resultant images represent an average over the 1-min scan to provide a stable reference measurement. Immediately after, a 3-dimensional pCASL sequence was run (*19*) (TR/TE, 3,720/22.9 ms; FoV, 208 × 208 mm^2; 16 slices; voxel size, 3.3 × 3.3 × 5.0 mm^3; postlabeling delay/labeling duration, 1,500/1,800 ms; label plane offset, 60 mm; 16 measurements). Lastly, proton density-weighted images were acquired by turning off the labeling or background suppression pulses (M_0; TR, 7,000 ms).

OxFlow images were analyzed following the approach outlined by Jain et al. (*14*). Briefly, regions of interest were semiautomatically drawn in and surrounding the vessels on the magnitude image, then transferred to the phase image to measure the mean phase difference in the feeding arteries, and between the sagittal sinus and the surrounding tissue. The pCASL images were motion corrected, coregistered to M_0, and smoothed with a 4-mm gaussian filter. CBF images were generated using the standard 1-compartment model (*12*). For this analysis, the blood–brain partition coefficient of water was 0.90 mL/g, the longitudinal relaxation time of blood was 1.65 s, and the labeling efficiency was assumed to be 0.86. Images were coregistered to the PET space using SPM12 (https://www.fil.ion.ucl.ac.uk/spm/).

PET-Only Imaging: DBFM

CBF (f_i) maps were generated from ^{15}O-H_2O PET by fitting the following equation to the local time–activity curves ($C_i(t)$):

$$C_i(t) = f_i \cdot C_a^w(t) * e^{-k_{2i}t} + V_{b_i}^w \cdot C_a^w(t), \qquad \text{Eq. 1}$$

where $*$ represents convolution. The fitting parameters were k_{2_i} (clearance rate constant), f_i, and $V_{b_i}^w$ (arterial blood volume). OEF (E_i) and $CMRO_2$ measurements were obtained by fitting ^{15}O-O_2 PET data to Equation 2 (*11*).

$$C_i(t) = E_i \cdot f_i \cdot A_o(t) * e^{-k_{2i}t} + f_i \cdot A_w(t) * e^{-k_{2i}t} + V_{0_i}^o \cdot A_o(t) + V_{A_i}^w \cdot A_w(t), \qquad \text{Eq. 2}$$

where $A_o(t)$ is the ^{15}O-O_2 component of the AIF. The fitting parameters were E_i, $V_{0_i}^o$ and $V_{A_i}^w$ (^{15}O-O_2 and ^{15}O-H_2O blood volumes, respectively). All fitting was performed in MATLAB using the optimization routine *fmincon*. $CMRO_2$ was calculated from Fick's principle as $CMRO_{2i} = E_i \cdot f_i \cdot C_aO_2$, where $C_aO_2 = 1.34 \cdot Hb \cdot S_aO_2 + 0.003 \cdot P_aO_2$, Hb is the hemoglobin

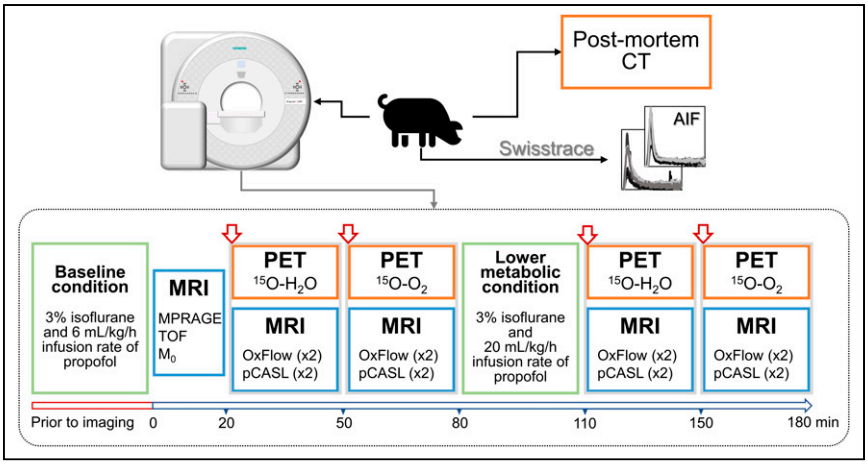

FIGURE 1. Protocol diagram showing imaging blocks acquired at baseline and under lower metabolic condition. Before imaging, animal was positioned in scanner and anesthetic was applied. At time zero, MRI was started, and onsite cyclotron was contacted to produce ^{15}O-H_2O dose, which was injected at 20-min mark. There was a delay of approximately 20 min before ^{15}O-O_2 delivery. After first ^{15}O-O_2 imaging block, propofol infusion rate was increased to 20 mL/kg/h.

concentration, and S_aO_2 (arterial saturation of oxygen) was estimated using the P_aO_2 (partial pressure of oxygen) measurements (*20*). A glossary of variables is provided in the supplemental data.

PMROx

PMROx $CMRO_2$ images were generated from ^{15}O-O_2 PET data using Equation 3, which was derived from the 1-tissue-compartment model (*9*).

$$CMRO_{2i} = CMRO_{2\mathrm{wb}} \left[\frac{\int_0^T C_i(t)dt + \frac{f_i}{p}\int_0^T \int_0^t C_i(u)dudt}{\int_0^T C_{\mathrm{wb}}(t)dt + \frac{f_{\mathrm{wb}}}{p}\int_0^T \int_0^t C_{\mathrm{wb}}(u)dudt} \right], \quad \text{Eq. 3}$$

where T is scan time. Local OEF was calculated by $E_i = CMRO_{2i}/(f_i \cdot C_aO_2)$. Both f_{wb} and $CMRO_{2\mathrm{wb}}$ were obtained from OxFlow, the latter by:

$$CMRO_{2\mathrm{wb}} = C_aO_2 \cdot f_{\mathrm{wb}} \left(\frac{S_aO_2 - S_vO_2}{S_aO_2} \right). \quad \text{Eq. 4}$$

CBF (Eq. 5) was obtained using the noninvasive PET/MR approach described by Ssali et al. (*10*), in which WB CBF is used to calibrate ^{15}O-H_2O PET data. In both Equations 3 and 5, WB $CMRO_2$, CBF, and time–activity curve are used as scalers to obtain the corresponding local values. Alternatively for CBF, a direct scaling approach could be implemented (*21*).

$$f_i = \frac{\int_0^T C_i(t)dt}{\frac{1}{f_{\mathrm{wb}}}\int_0^T C_{\mathrm{wb}}(t)dt + \frac{1}{p}\left(\int_0^T \int_0^t C_{\mathrm{wb}}(u)dudt - \int_0^T \int_0^t C_i(u)dudt\right)}. \quad \text{Eq. 5}$$

The feasibility of implementing pCASL into the PMROx approach ($PMROx_{ASL}$) was also evaluated. In this case, f_i in Equation 3 was obtained from the CBF images generated by pCASL.

Regional CBF, OEF and $CMRO_2$ Measurements

Volumes of interest (VOIs) were semiautomatically drawn on the MPRAGE images for each animal and then transferred to the corresponding CBF, OEF and $CMRO_2$ images. Measurements were made for cerebellum (4.2 ± 0.7 cm^3); diencephalon (4.7 ± 0.6 cm^3); and frontal (2.4 ± 0.6 cm^3), occipital (7.9 ± 1.5 cm^3), parietal (9.1 ± 1.6 cm^3), and temporal (6.0 ± 0.6 cm^3) lobes. All images were registered to the anatomic image of 1 animal to generate groupwise maps using SPM12.

Statistics

Local measurements were compared using linear regression to obtain the Pearson correlation coefficient (ρ). Any potential bias was assessed using a 1-sample t test. Paired t tests were performed to evaluate differences between measurements. Statistical significance was defined by $P < 0.05$, and Bonferroni adjustment was performed when necessary. Measurements are expressed in terms of mean ± SD. Statistical tests were performed using SPSS (version 26, https://www.ibm.com/analytics/spss-statistics-software).

RESULTS

Data from 9 juvenile pigs were collected (age range, 8–10 wk; weight, 19 ± 2 kg; 5 female). In 1 experiment, only ^{15}O-H_2O data were acquired due to a technical issue with the ^{15}O oxygen line. The LMC was successfully induced in 6 animals. Supplemental Table 1 provides a summary of arterial blood measurements during baseline and LMC.

AIFs could not be acquired in 3 cases (1 ^{15}O-H_2O and 2 ^{15}O-O_2) due to clotting of the sampling line. In these cases, population-based AIFs were used after using a scaling factor for each animal individually. For the ^{15}O-H_2O case, the AIF was scaled by the injected dose (MBq). Because the administered activity was unknown for ^{15}O-O_2, the AIF was scaled to the mean jaw muscle activity (C_m) measured from a 50-mm^2 ROI. The appropriate scaling factor was determined by a combination of principal component and multiple linear regression analyses involving the remaining 6 measured AIFs. The factors included body weight (kg), endotracheal tube peak activity (kBq/mL), mean jaw muscle activity concentration (kBq/mL), and partial pressure of carbon dioxide (mm Hg). The resulting model equation was subsequently used to scale the population-based AIF for each animal. Principal component analysis and multiple linear regression identified mean jaw muscle activity concentration (C_m) as a significant component for estimating the scaling factor of ^{15}O-O_2 ($=43.5 \cdot C_m$; $R^2 = 0.998$). Supplemental Figure 2 presents a comparison between ^{15}O-O_2–measured AIFs with their respective scaled population-based curves; the blue curves represent the population-based AIFs used for the 2 animals for which arterial sampling failed.

Validation

Average WB estimates of CBF, OEF and $CMRO_2$ from PET and PET/MR were in good agreement, with no significant differences between techniques: 56.6 ± 21.0 mL/100 g/min, 0.31 ± 0.09, and 1.81 ± 0.10 mLO_2/100 g/min from DBFM and 54.1 ± 16.7 mL/100 g/min, 0.30 ± 0.09, and 1.89 ± 0.16 mLO_2/100 g/min from

OxFlow/PMROx, respectively. Average WB-V_b^w from ^{15}O-H_2O PET was 9.5 ± 4.0 mL/100 g, and WB V_0^o and V_A^w values from ^{15}O-O_2 PET were 7.0 ± 1.0 mL/100 g and 2.6 ± 6.7 mL/100 g, respectively. WB V_A^w was small (<2 mL/100 g) for 7 of 8 animals; however, in 1 outlier it was 19.1 mL/100 g.

Regional results of regression and correlation (Fig. 2) analyses from CBF, OEF, and $CMRO_2$ measurements are summarized in Table 1. Significant correlations between regional CBF estimates from noninvasive PET/MR and DBFM were observed in all VOIs. The Bland–Altman plot indicated a bias in local CBF measurements by noninvasive PET/MR for the parietal lobe (7.7 mL/100 g/min, $P = 0.02$) and diencephalon (14.8 mL/100 g/min, $P = 0.02$). Strong correlations between regional OEF estimates from PMROx and DBFM were observed (Figs. 2B and 3). Finally, regression between $CMRO_2$ estimates from the 2 techniques revealed good agreement, with a moderate correlation and a small bias in the PMROx measurements for the cerebellum (0.16 mLO_2/100 g/min, $P = 0.03$) and diencephalon (0.30 mLO_2/100 g/min, $P < 0.01$).

PMROx$_{ASL}$

Average WB estimates of CBF and $CMRO_2$ from pCASL and PMROx$_{ASL}$ were 58.6 ± 20.4 mL/100 g/min and 1.88 ± 0.24 mLO_2/100 g/min, respectively, which were not significantly different from the PET-only results. Regional measurements were successfully extracted from all VOIs (Table 1; Figs. 3 and 4), except for the cerebellum from 1 animal because this region was missing in the pCASL FoV. Strong correlations between DBFM and pCASL CBF estimates were observed, as well as between DBFM and PMROx$_{ASL}$ OEF estimates, with a small bias in the temporal lobe (–0.048, $P = 0.02$). $CMRO_2$ values from PMROx$_{ASL}$ and DBFM showed a moderate correlation.

Lower Metabolic Condition

For the 6 animals in which measurements were acquired under both conditions, propofol caused WB CBF to decrease to 27.3 ± 7.0 and 29.9 ± 6.4 mL/100 g/min for OxFlow and pCASL, respectively (50% reduction; Figs. 3 and 5A). There was a corresponding significant increase in OEF of 0.11 ± 0.06 (Fig. 5B) measured by OxFlow, and a significant reduction in WB-$CMRO_2$ measured by PMROx and PMROx$_{ASL}$ of 0.68 ± 0.36 and 0.67 ± 0.36 mLO_2/100 g/min, respectively (Figs. 3 and 5C).

DISCUSSION

^{15}O-O_2 PET has been used extensively to assess disruptions in cerebral energy metabolism, such as after stroke, predicting its risk of recurrence, and understanding energy regulation during functional activation (*22*). Despite the proven value of ^{15}O-O_2 PET, the procedure is complex and invasive, which has led to a diminishing number of sites with the necessary expertise to conduct ^{15}O-O_2 studies. This trend highlights the value to develop simpler ^{15}O-O_2 imaging protocols that retain the inherent quantitative capabilities of PET. This study focused on validating a hybrid PET/MR technique developed specifically to address this issue. The possibility of using PET/

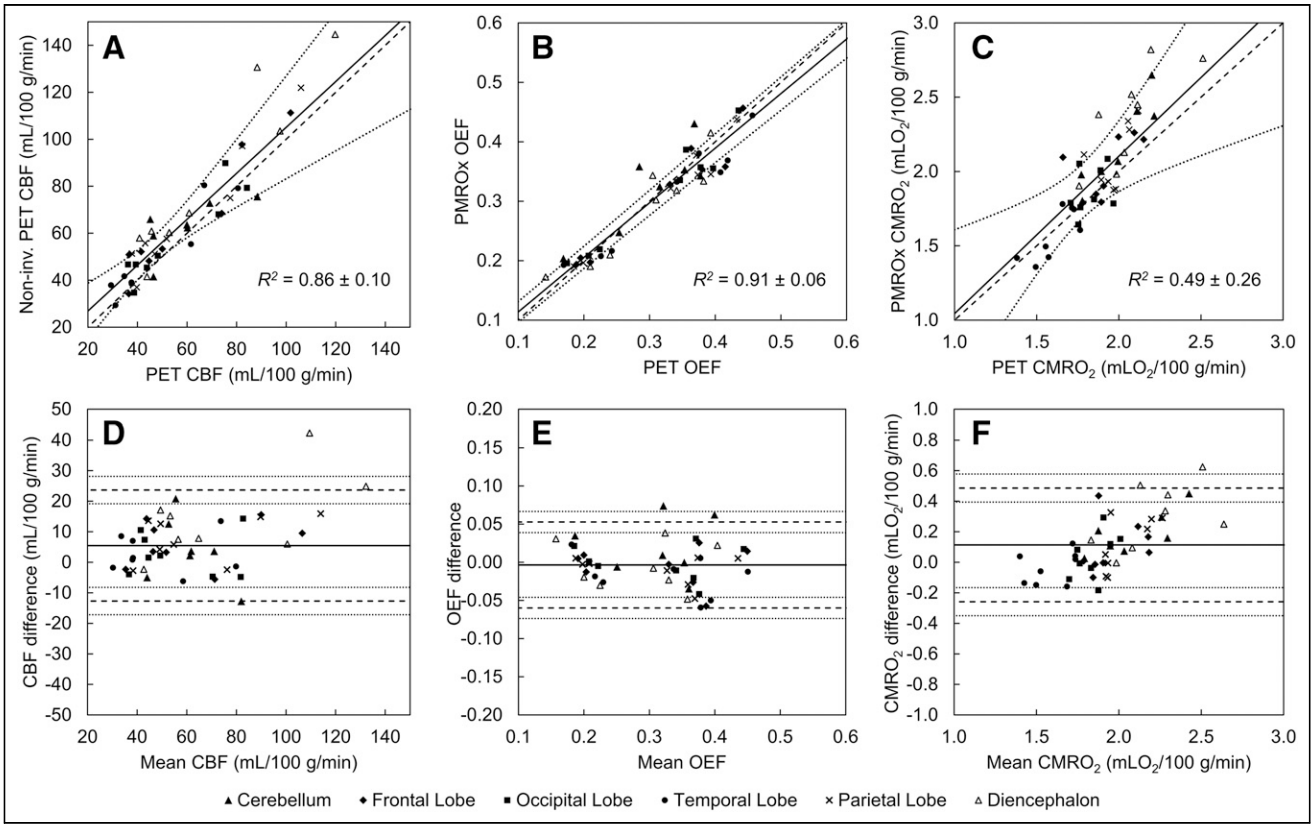

FIGURE 2. (A) Local baseline CBF from noninvasive PET/MR and DBFM. Average regression line is represented by solid line ($y = 0.98x + 7.29$; 95% confidence interval [CI] is represented by dotted lines). Dashed line is identity line. Corresponding OEF (B) and $CMRO_2$ (C) results presented average regression line of $y = 0.92x + 0.02$ and $y = 1.06x - 0.02$, respectively. Bland–Altman plots from corresponding data are presented in D–F, where mean is represented by solid line. Dashed lines represent limits of agreement (±2 SD), each with its 95% CI (dotted lines). Mean difference for all VOIs was 6.2 mL/100 g/min for CBF, −0.004 for OEF, and 0.12 mLO_2/100 g/min for $CMRO_2$.

TABLE 1
Summary of Regression and Correlation Analyses Performed on Local Baseline Measurements ($n = 8$) of CBF (mL/100 g/min), OEF, and $CMRO_2$ (mLO_2/100 g/min)

Technique	Measurement	Slope	Intercept	ρ
PMROx	CBF	0.98 ± 0.20	7.3 ± 9.8	0.91 ± 0.10
	OEF	0.92 ± 0.03*	0.02 ± 0.01†	0.95 ± 0.04
	$CMRO_2$	1.06 ± 0.35	−0.02 ± 0.63	0.67 ± 0.20
$PMROx_{ASL}$	CBF	0.85 ± 0.15	10.9 ± 11.7	0.80 ± 0.18
	OEF	0.83 ± 0.13*	0.05 ± 0.03†	0.87 ± 0.09
	$CMRO_2$	1.15 ± 0.41	−0.16 ± 0.70	0.53 ± 0.14

*Significantly different from one.
†Significantly different from zero.

MR to update ^{15}O-O_2 imaging was investigated by Su et al., who used MRI to extract image-derived AIFs (*8*). The current study explored an alternative approach using WB MRI measurements as a reference, which avoids potential registration and partial-volume errors. PMROx is also less sensitive to errors caused by RW and the CBV since regional $CMRO_2$ is determined from the ratio of time–activity curves.

Validation experiments were conducted using a porcine model and involved imaging $CMRO_2$ independently using the previously validated DBFM (*11*). For this method, an MR-compatible arterial sampling system was used to measure the AIF for both tracers. Good agreement between PMROx and DBFM was found across VOIs with respect to both OEF and $CMRO_2$, although a small bias was observed in the PMROx $CMRO_2$ estimates (Fig. 2F). Regression analysis also demonstrated strong and moderate correlations between techniques for OEF and $CMRO_2$, respectively. The lower correlation for the latter is explained by its dependency on both OEF and CBF. In addition to the agreement with DBFM, PMROx was shown to be sensitive to reduced energy metabolism caused by increasing the propofol infusion. The $CMRO_2$ reduction was driven by the propofol-induced decrease in CBF, since propofol caused an increase in OEF. These findings are in agreement with Oshima et al. who reported that propofol caused proportional decreases in CBF and $CMRO_2$ but had no effect on the arteriovenous oxygen difference (*23*).

Because the PMROx approach scales the ^{15}O-O_2 images by an MRI estimate of WB $CMRO_2$, its accuracy and precision will be directly affected by the MRI methods used to calculate WB OEF and CBF. In this study, WB OEF and $CMRO_2$ were measured by OxFlow, which can be acquired with scan times as short as 8 s with reproducibility of 2% for S_vO_2 and 6% for WB $CMRO_2$ (*24*). The accuracy of OxFlow depends on positioning the slices

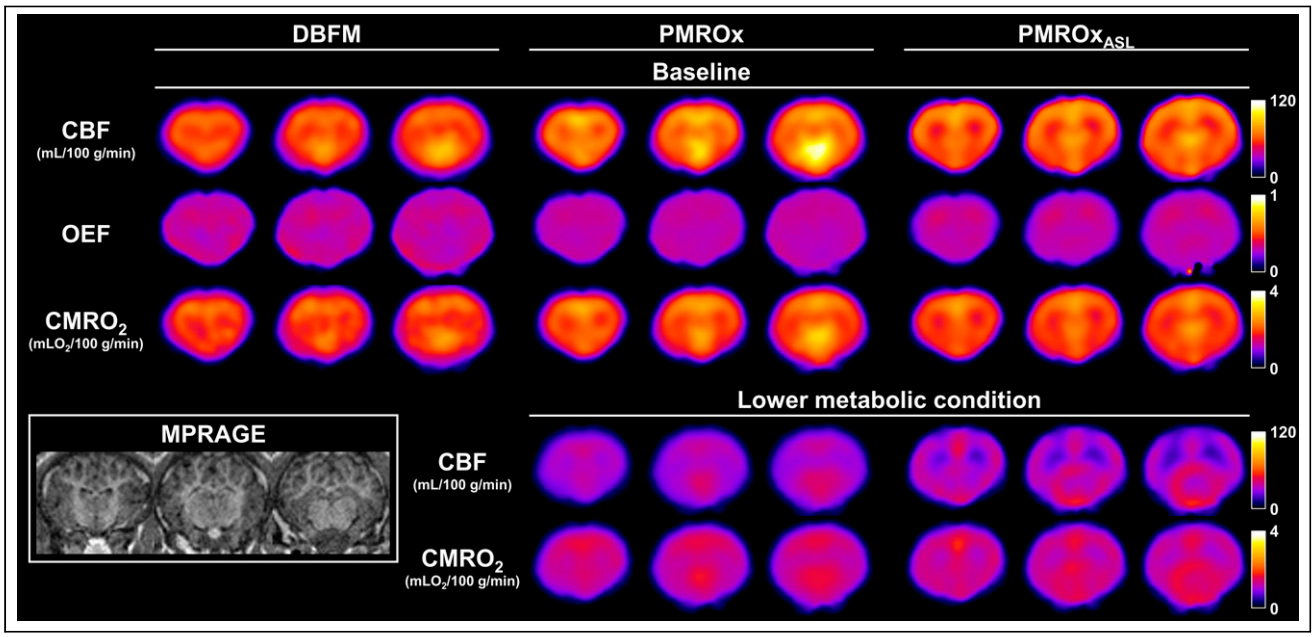

FIGURE 3. Groupwise CBF, OEF, and $CMRO_2$ images obtained with DBFM, PMROx, and $PMROx_{ASL}$ techniques for baseline ($n = 8$, top 3 rows). CBF and $CMRO_2$ results from PMROx and $PMROx_{ASL}$ for lower metabolic condition ($n = 6$) are presented on bottom 2 rows. MPRAGE from 1 animal was included for anatomic reference.

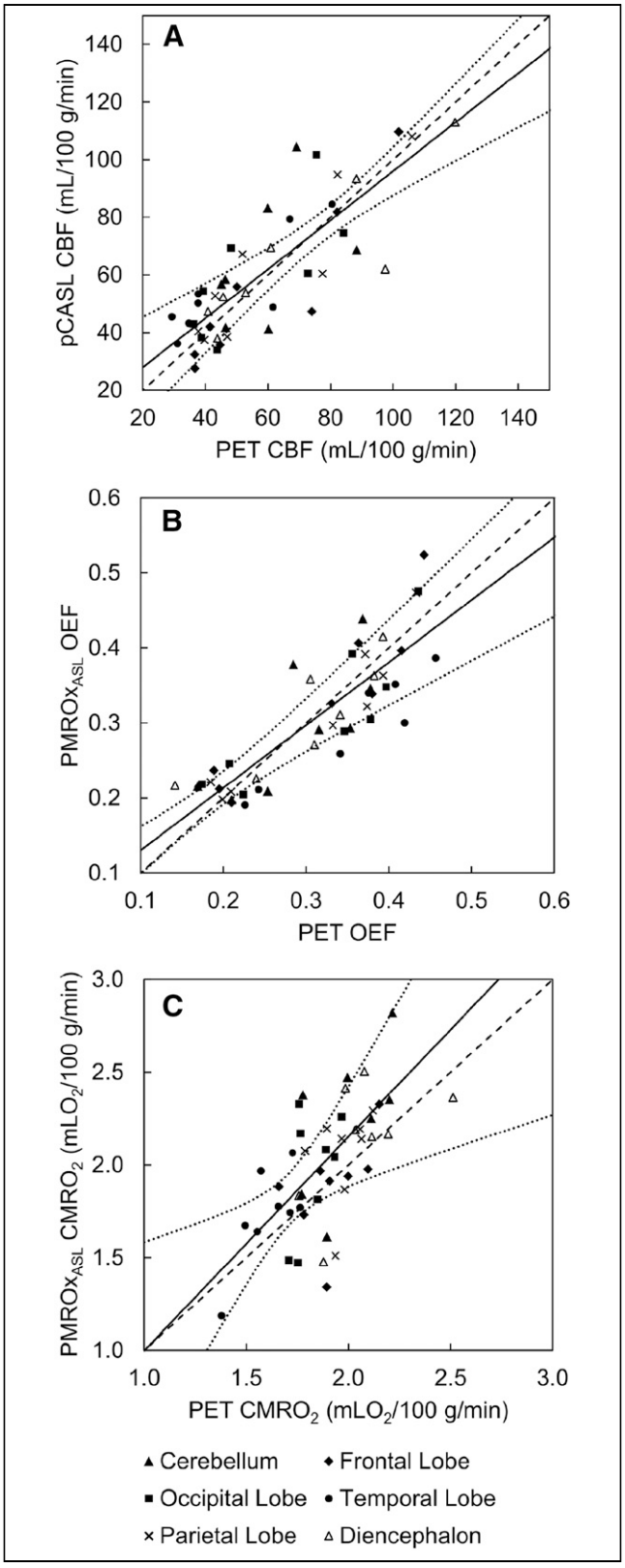

FIGURE 4. (A) Local baseline CBF from pCASL and DBFM. Average regression line is represented by solid line ($y = 0.85x + 10.91$; 95% confidence interval [CI] is represented by dotted lines). Dashed line is identity line. Corresponding OEF (B) and $CMRO_2$ (C) results presented average regression line of $y = 0.83x + 0.05$ and $y = 1.15x - 0.16$, respectively.

orthogonally to the main magnetic field, correcting for magnetic field inhomogeneities, and using sufficient image resolution to avoid partial-volume effects (*13*). The current study presents, to our knowledge, the first simultaneous comparison of OxFlow to ^{15}O-H_2O and ^{15}O-O_2 PET, and no significant differences were found between techniques. This agreement is in accordance with 2 recent studies comparing MR measurements of S_vO_2 with either PET or direct measures from the jugular blub (*25*,*26*).

PET/MR also provides the possibility of reducing the PET procedure to just ^{15}O-O_2 inhalation by replacing ^{15}O-H_2O PET with ASL ($PMROx_{ASL}$). WB CBF estimates from pCASL were in good agreement to those obtained by ^{15}O-H_2O PET, similar to previous ASL/PET comparisons conducted using a swine model (*10*,*27*). Strong correlations between regional CBF measurements were found for all VOIs except the cerebellum, which was attributed to limited spatial coverage for the pCASL sequence. Recent studies comparing ASL with PET involving human participants indicate that ASL can provide accurate CBF measurements with careful attention to common sources of error (*28*), including low signal-to-noise ratio and sensitivity to transit times (*29*). Consequently, translation to clinical studies remains an active area of research as factors such as cerebrovascular disease and ageing can impact its accuracy (*30*).

A challenge with PET-only imaging is correcting for signal contamination from the CBV (*4*). Blood volume terms were incorporated into the fitting procedure for both tracers. Although the average V_b^w was larger than reported in human studies, it is in accordance with Olsen et al. who reported values from 9 to 18 mL/100 g in pigs, depending on partial pressures of carbon dioxide levels (*31*). The V_0^o values were smaller because they are scaled by OEF and the venous fraction. WB V_A^w estimates were very small for most animals, as expected, as it only becomes significant in highly vascularized regions (*11*). In 1 animal, V_A^w reached a nonphysiologic value, which was likely a result of estimating $A_w(t)$ using a physiologic model.

Although this study demonstrated the advantages of PET/MRI for imaging $CMRO_2$ (*32*), this modality is not widely accessible and requires an onsite cyclotron for ^{15}O-O_2 production. A potential limitation with the current study was the indirect methods used to account for RW and CBV in the DBFM, rather than direct measurements; however, this approach has been previously validated (*11*). Lastly, Figure 2F indicates that the discrepancy between PMROx and DBFM increased as the difference between local and WB OEF values increased, which is attributed to neglecting RW by PMROx. It should be possible to reduce this error by incorporating an RW term in the model equation (*9*).

CONCLUSION

This study presents the validation of a noninvasive hybrid PET/MR technique to image $CMRO_2$ that requires a short inhalation of ^{15}O-O_2, followed by 5 min of PET and simultaneous MRI. Good agreement between $CMRO_2$ values from PMROx and the DBFM was found, and the proposed method was shown to be sensitive to reduced cerebral metabolism induced by increasing the anesthetic level.

DISCLOSURE

This work was supported by the Canadian Institutes of Health Research, grant 148600. No other potential conflict of interest relevant to this article was reported.

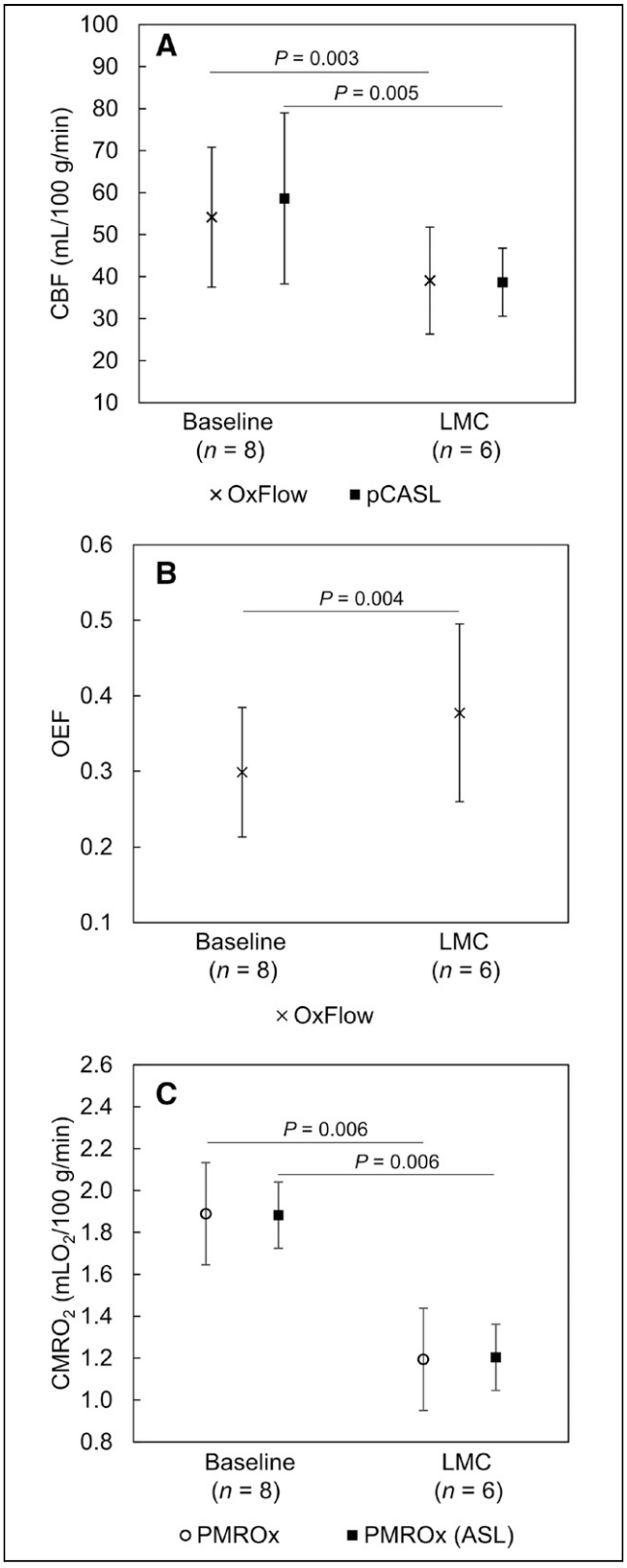

FIGURE 5. WB CBF (A), OEF (B), and $CMRO_2$ (C) values for baseline and LMC. Significant reductions in WB-CBF and WB-$CMRO_2$ were observed for both techniques, whereas significant increase was observed for WB-OEF.

KEY POINTS

QUESTION: Can the $CMRO_2$ be quantified using MRI functional measurements to calibrate ^{15}O-O_2 PET?

PERTINENT FINDINGS: The proposed PMROx approach resulted in $CMRO_2$ values comparable to those obtained from a PET-only technique. PMROx was further simplified by incorporating ASL, and it proved sensitive to anesthetic-induced changes in metabolism.

IMPLICATIONS FOR PATIENT CARE: PMROx is a noninvasive technique that requires only ^{15}O-O_2, which facilitates its application in human studies, and it may prove to be a useful tool to better understand disorders characterized by disruptions in the cerebral oxidative metabolism.

REFERENCES

1. Lin W, Powers WJ. Oxygen metabolism in acute ischemic stroke. *J Cereb Blood Flow Metab.* 2018;38:1481–1499.
2. Vaishnavi SN, Vlassenko AG, Rundle MM, Snyder AZ, Mintun MA, Raichle ME. Regional aerobic glycolysis in the human brain. *Proc Natl Acad Sci USA.* 2010; 107:17757–17762.
3. Baron JC, Jones T. Oxygen metabolism, oxygen extraction and positron emission tomography: historical perspective and impact on basic and clinical neuroscience. *Neuroimage.* 2012;61:492–504.
4. Mintun MA, Raichle ME, Martin WR, Herscovitch P. Brain oxygen utilization measured with O-15 radiotracers and positron emission tomography. *J Nucl Med.* 1984; 25:177–187.
5. Kudomi N, Hayashi T, Teramoto N, et al. Rapid quantitative measurement of CMRO2 and CBF by dual administration of 15O-labeled oxygen and water during a single PET scan: a validation study and error analysis in anesthetized monkeys. *J Cereb Blood Flow Metab.* 2005;25:1209–1224.
6. Ohta S, Meyer E, Thompson CJ, Gjedde A. Oxygen consumption of the living human brain measured after a single inhalation of positron emitting oxygen. *J Cereb Blood Flow Metab.* 1992;12:179–192.
7. Kudomi N, Maeda Y, Yamamoto H, Yamamoto Y, Hatakeyama T, Nishiyama Y. Reconstruction of input functions from a dynamic PET image with sequential administration of 15O2 and H215O for noninvasive and ultra-rapid measurement of CBF, OEF, and CMRO2. *J Cereb Blood Flow Metab.* 2018;38:780–792.
8. Su Y, Vlassenko AG, Couture LE, et al. Quantitative hemodynamic PET imaging using image-derived arterial input function and a PET/MR hybrid scanner. *J Cereb Blood Flow Metab.* 2017;37:1435–1446.
9. Narciso L, Ssali T, Iida H, St Lawrence K. A non-invasive reference-based method for imaging the cerebral metabolic rate of oxygen by PET/MR: theory and error analysis. *Phys Med Biol.* 2021;66:065009.
10. Ssali T, Anazodo UC, Thiessen JD, Prato FS, St. Lawrence K. A noninvasive method for quantifying cerebral blood flow by hybrid PET/MRI. *J Nucl Med.* 2018;59:1329–1334.
11. Kudomi N, Hirano Y, Koshino K, et al. Rapid quantitative CBF and CMRO2 measurements from a single PET scan with sequential administration of dual ^{15}O-labeled tracers. *J Cereb Blood Flow Metab.* 2013;33:440–448.
12. Alsop DC, Detre JA, Golay X, et al. Recommended implementation of arterial spin-labeled perfusion MRI for clinical applications: a consensus of the ISMRM perfusion study group and the European consortium for ASL in dementia. *Magn Reson Med.* 2015;73:102–116.
13. Wehrli FW, Rodgers ZB, Jain V, et al. Time-resolved MRI oximetry for quantifying CMRO2 and vascular reactivity. *Acad Radiol.* 2014;21:207–214.
14. Jain V, Langham MC, Wehrli FW. MRI estimation of global brain oxygen consumption rate. *J Cereb Blood Flow Metab.* 2010;30:1598–1607.
15. Cockburn N, Corsaut J, Kovacs MS, St. Lawrence K, Hicks JW. Validation protocol for current good manufacturing practices production of [^{15}O]water for hybrid PET/MR studies. *Nucl Med Commun.* 2020;41:1100–1105.
16. Iguchi S, Moriguchi T, Yamazaki M, et al. System evaluation of automated production and inhalation of ^{15}O-labeled gaseous radiopharmaceuticals for the rapid ^{15}O-oxygen PET examinations. *EJNMMI Phys.* 2018;5:37.

17. Hori Y, Hirano Y, Koshino K, et al. Validity of using a 3-dimensional PET scanner during inhalation of 15 O-labeled oxygen for quantitative assessment of regional metabolic rate of oxygen in man. *Phys Med Biol.* 2014;59:5593–5609.
18. Kudomi N, Hayashi T, Watabe H, et al. A physiologic model for recirculation water correction in CMRO2 assessment with 15O2 inhalation PET. *J Cereb Blood Flow Metab.* 2009;29:355–364.
19. Günther M, Oshio K, Feinberg DA. Single-shot 3D imaging techniques improve arterial spin labeling perfusion measurements. *Magn Reson Med.* 2005;54:491–498.
20. Severinghaus JW. Simple, accurate equations for human blood O2 dissociation computations. *J Appl Physiol.* 1979;46:599–602.
21. Ishii Y, Thamm T, Guo J, et al. Simultaneous phase-contrast MRI and PET for noninvasive quantification of cerebral blood flow and reactivity in healthy subjects and patients with cerebrovascular disease. *J Magn Reson Imaging.* 2020;51:183–194.
22. Vafaee MS, Vang K, Bergersen LH, Gjedde A. Oxygen consumption and blood flow coupling in human motor cortex during intense finger tapping: Implication for a role of lactate. *J Cereb Blood Flow Metab.* 2012;32:1859–1868.
23. Oshima T, Karasawa F, Satoh T. Effects of propofol on cerebral blood flow and the metabolic rate of oxygen in humans. *Acta Anaesthesiol Scand.* 2002;46:831–835.
24. Barhoum S, Langham MC, Magland JF, et al. Method for rapid MRI quantification of global cerebral metabolic rate of oxygen. *J Cereb Blood Flow Metab.* 2015;35:1616–1622.
25. Miao X, Nayak KS, Wood JC. In vivo validation of T2- and susceptibility-based SvO2 measurements with jugular vein catheterization under hypoxia and hypercapnia. *Magn Reson Med.* 2019;82:2188–2198.
26. Jiang D, Deng S, Franklin CG, et al. Validation of T2-based oxygen extraction fraction measurement with ^{15}O positron emission tomography. *Magn Reson Med.* 2021;85:290–297.
27. Andersen JB, Henning WS, Lindberg U, et al. Positron emission tomography/magnetic resonance hybrid scanner imaging of cerebral blood flow using ^{15}O-water positron emission tomography and arterial spin labeling magnetic resonance imaging in newborn piglets. *J Cereb Blood Flow Metab.* 2015;35:1703–1710.
28. Puig O, Henriksen OM, Vestergaard MB, et al. Comparison of simultaneous arterial spin labeling MRI and ^{15}O-H2O PET measurements of regional cerebral blood flow in rest and altered perfusion states. *J Cereb Blood Flow Metab.* 2020;40:1621–1633.
29. Wu WC, St Lawrence KS, Licht DJ, Wang DJJ. Quantification issues in arterial spin labeling perfusion magnetic resonance imaging. *Top Magn Reson Imaging.* 2010;21:65–73.
30. Fan AP, Jahanian H, Holdsworth SJ, Zaharchuk G. Comparison of cerebral blood flow measurement with [^{15}O]-water positron emission tomography and arterial spin labeling magnetic resonance imaging: a systematic review. *J Cereb Blood Flow Metab.* 2016;36:842–861.
31. Olsen AK, Keiding S, Munk OL. Effect of hypercapnia on cerebral blood flow and blood volume in pigs studied by positron emission tomography. *Comp Med.* 2006;56:416–420.
32. Fan AP, An H, Moradi F, et al. Quantification of brain oxygen extraction and metabolism with [^{15}O]-gas PET: a technical review in the era of PET/MRI. *Neuroimage.* 2020;220:117136.